NANO LETTERS

Letter

pubs.acs.org/NanoLett

Tunable Photoemission from an Excitonic Antitrap

Katarzyna Kowalik-Seidl,*[,†] Xaver P. Vögele,[†] Bernhard N. Rimpfl,[†] Georg J. Schinner,[†] Dieter Schuh,[‡] Werner Wegscheider,[§] Alexander W. Holleitner,[∥] and Jörg P. Kotthaus[†]

[†]Fakultät für Physik and Center for NanoScience (CeNS), Ludwig-Maximilians-Universität, Geschwister-Scholl-Platz 1, D-80539 München, Germany

[‡]Institut für Experimentelle und Angewandte Physik, Universität Regensburg, Universitätsstraße 31, D-93053 Regensburg, Germany

[§]Laboratorium für Festkörperphysik, HPF E 7, ETH Zürich, Schafmattstr. 16, 8093 Zürich, Switzerland

[∥]Walter Schottky Institut and Physik-Department, Technische Universität München, Am Coulombwall 4a, D-85748 Garching, Germany

Supporting Information

ABSTRACT: We study the influence of lithographically defined, electrostatic trap configurations on the photon emission from dipolar excitons in coupled quantum wells. The emission is surprisingly enhanced for an excitonic antitrap compared to a trap configuration, an effect more pronounced for a trap with smaller diameter. We explain the observations by the interplay between the exciton formation process, the lateral charge-carrier dynamics, and the dipole−dipole interactions between the excitons. Exploiting this interplay allows us to efficiently tune the excitonic emission energy with very small intensity variation.

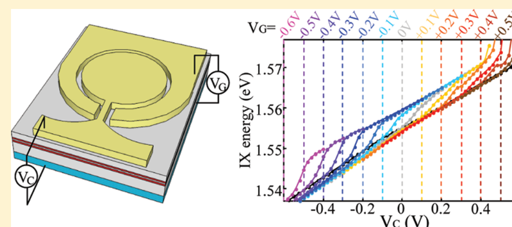

KEYWORDS: *Dipolar exciton, exciton trap, exciton antitrap, electro-optical modulator*

Traps for dipolar excitons, generated in semiconductor double quantum wells, are subject of current research on both a fundamental level and for potential electro-optic applications. The widely tunable recombination lifetime of such excitons enables the formation of excitonic ensembles with varying density. Therefore, these excitons are ideal composite particles for studies of potential Bose−Einstein condensation (BEC).[1,2] Different methods to spatially confine dipolar excitons have been realized, either by using aleatory traps created at the quantum wells' interfaces[3] or by building stress-induced,[4] magnetic,[5] and electrostatic traps.[6−10] In comparison, electrostatic traps are highly advantageous because of their facile tunability. Gated structures for controlling dipolar excitons are also investigated for their potential applications in electro-optic devices, and so far the following have been demonstrated: (i) the controlled storage of excitons (photonic memories),[11−13] (ii) spin memory coded in the exciton polarization,[14,15] and (iii) basic logical operations with micrometer size exciton circuits.[16−18] For realizing such devices on a submicrometer or even nanoscale dimension, lateral electric fields between two adjacent gates need to be considered.[19] Hereby, lateral escape dynamics of photo-generated charge-carriers become important, and typically it is assumed that these hinder the functioning of effective exciton traps and devices.

In this Letter, we demonstrate that such charge-carrier dynamics can be tailored in a way that the overall photon emission out of an excitonic trapping potential is efficiently enhanced. We present photoluminescence emission studies of dipolar excitons from both an electrostatically defined trapping and antitrapping potential measured in a confocal geometry with the 1 μm resolution.[15] The excitonic emission is surprisingly enhanced for the excitonic antitrap compared to the trap configuration. The reason for this counterintuitive behavior is a competition of processes determining the eventual excitonic photon emission. These are the exciton formation, the dipole−dipole interaction between the excitons, and the lateral escape dynamics of both electrons and holes in the trapping and antitrapping potentials. We verify that the energy of the emitted photons is widely tunable at fairly constant emission intensity when these processes are balanced. Intriguingly, the resulting photoluminescence emission and tunability are even more pronounced for a smaller trap size. Hereby, our device concept may prove useful for energy modulation or wavelength division multiplexing interconnections in nanoscale excitonic circuits.[20]

Figure 1a sketches the geometry of the devices defined on a GaAs/AlGaAs heterostructure. A central surface gate (C-gate) is surrounded by a guard gate (G-gate). We show data from two different devices with C-gate diameters of 23.4 μm (device T1) and 16.5 μm (device T2) (see Supporting Information Section S1 for device details). Applying a voltage V_C to the C-gate with respect to a back gate produces a band tilting in the semiconductor heterostructure below the gate. In turn, spatially indirect excitons (IX) become energetically favorable at this

Received: October 13, 2011
Revised: December 2, 2011
Published: December 5, 2011

 © 2011 American Chemical Society

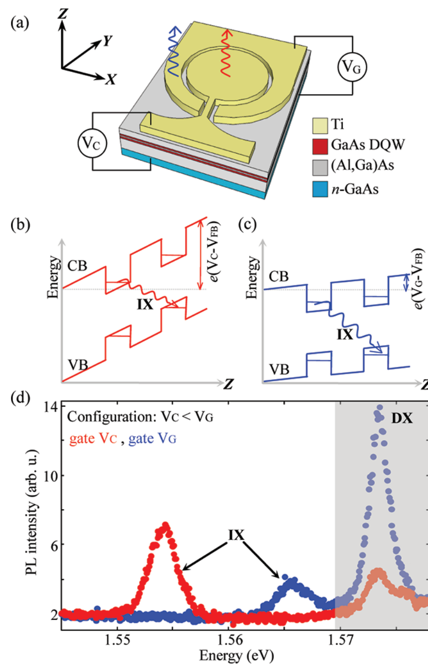

Figure 1. (a) Sketch of the trapping/antitrapping devices. Yellow: central gate C-gate with the surrounding guard gate G-gate. (b,c) Sketch of the conduction and valence band along the growth direction Z below the C- and G-gate ($V_C < V_G < V_{FB}$). The applied gate voltage V_G (V_C) and built-in voltage V_{FB} sum up to an electric field between the n-doped back gate and the top G(C)-gate. (d) Photoluminescence spectra of DX and IX excitons measured at the position of the G-gate (blue) and C-gate (red) of device T1 for $V_G = +0.3$ V, $V_C = 0$ V, and $T = 4.2$ K .

position in the coupled quantum well (Figure 1b). Such excitons are dipolar, since their constituting electrons and holes are located in different quantum wells, separated by a high energy barrier. Equally, indirect excitons are trapped below the G-gate, and their energy is influenced by voltage V_G (Figure 1c). Both surface gates are made of Ti. Neglecting screening by net charges between the top and back gate, the effective electric field perpendicular to the CQW is given by $F_{C(G)} = -(V_{C(G)} - V_{FB})/a$, where a is the distance between the top- and back gate (370 nm). The voltage V_{FB} is the flat band voltage reflecting the built-in electric field caused by charged states at the GaAs-metal interface. For $V_C < V_G < V_{FB}$, the indirect excitons below the C-gate have a lower energy than the ones below the G-gate. This can be verified by photoluminescence spectra taken at positions of the C-gate and G-gate (red and blue curves in Figure 1d). Therefore, for $V_C < V_G < V_{FB}$ a trap for indirect excitons is realized below the C-gate. For $V_G < V_C < V_{FB}$, however, an antitrap is formed, because then indirect excitons have a lower energy below the G-gate. The photoluminescence resonances at ~1.574 eV in Figure 1d stem from excitons which are located in just one quantum well. The photoluminescence energy of such direct excitons (DX) depends much less on the electric Stark fields, acting perpendicular to the CQW plane, than for indirect excitons, because of their smaller dipole moment.[21]

Figure 2a sketches the in-plane variation of the excitonic potential for the trap (solid line) and antitrap configuration (dashed line). At first glance, it seems a paradox to expect less excitonic emission from the trap than from the antitrap. However, particularly for the confocal arrangement of the excitation and detection one needs to consider the lateral

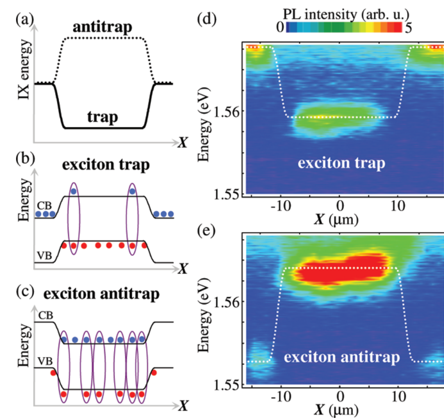

Figure 2. (a) Sketch of the IX energy versus X-spatial coordinate for exciton trap (solid line) and antitrap (dotted line). (b) Conduction and valence band evolution for the trap ($V_C < V_G$) and (c) antitrap configuration ($V_C > V_G$). Blue and red points represent photogenerated free electrons and holes. Ovals indicate formed excitons. (d,e) Color-encoded photoluminescence intensity and energy of indirect excitons along the C-gate diameter of device T1 in the X-direction for two voltage configurations: (d) exciton trap with $V_C = 0$ V, $V_G = +0.2$ V and (e) exciton antitrap with $V_C = 0$ V, $V_G = -0.2$ V. White dotted lines sketch the trap/antitrap potential for indirect excitons.

dynamics of photogenerated electrons and holes before they form indirect excitons as well.[22] In the trap configuration with $V_C < V_G$, photogenerated holes are confined below the C-gate, and the energetically favorable state for electrons is below the G-gate (Figure 2b). In analogy, an excitonic antitrap with $V_G < V_C$ favors the localization of electrons (holes) below the C-gate (G-gate) (Figure 2c). The diffusivity and mobility is larger for electrons than for holes in GaAs. Hereby, more electrons can escape in the trap situation (Figure 2b) than holes in the antitrap configuration (Figure 2c). Then, the imbalance of photogenerated electrons and holes is less for the antitrap compared to the trap configuration. In turn, a larger number of excitons can be eventually formed in the antitrap (ovals in Figure 2b,c). We experimentally verify both scenarios by characterizing the trapping and antitrapping potentials by a confocal photoluminescence experiment.[23] Figure 2d,e depicts the photoluminescence measured along the X-direction across device T1 (see Supporting Information Sections S2 and S3 for details on the experiment). We would like to point out the following. For the trap configuration (Figure 2d), we detect emission from indirect excitons only from the area of the C-gate, and the emission energy is lower than for the antitrap (Figure 2e). These findings prove the formation of an effective trap in the situation of Figure 2d. The emission intensity from the area of the C-gate for the antitrap situation (Figure 2e), however, is enhanced compared to the trap configuration. Intriguingly, for the antitrap the photoluminescence intensity below the C-gate is even larger than below the G-gate.

To further analyze the electro-optic phenomenon, we record the photoluminescence intensity from the C-gate of device T1 when V_C is continuously swept at a fixed V_G. Hereby, we cross from the trap to the antitrap situation (Figure 3a). On the one hand, we detect a linear Stark-shift of the emission energy with a ratio of $\Delta E/\Delta V_C \sim 30$ meV/V in both trapping and antitrapping configurations (dotted lines in Figure 3a), which is in agreement with earlier reports.[24,22] On the other hand, $\Delta E/\Delta V_C$ is few times enhanced for the voltage regime

dx.doi.org/10.1021/nl203613k | Nano Lett. 2012, 12, 326−330

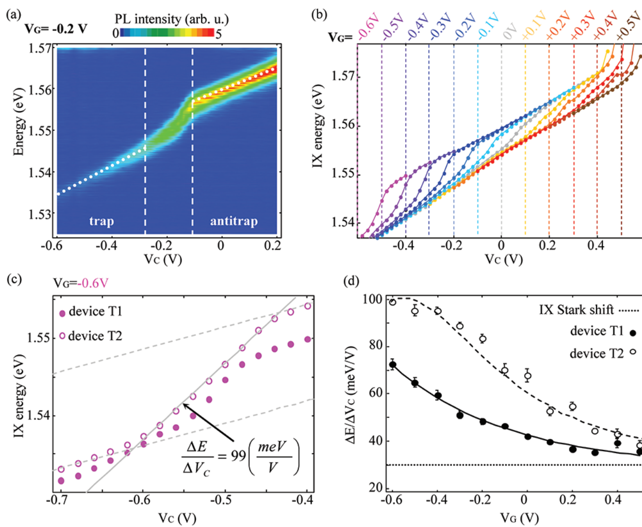

Figure 3. Photoluminescence energy of indirect excitons at position of the C-gate as function of V_C at $V_G = -0.2$ V. Color encodes the emission intensity. Dashed vertical lines mark the transition of the trap–antitrap configuration. Dotted lines highlight the linear Stark shift in the trap (left) and antitrap (right) configuration. (b) Fitted energy of the indirect exciton photoluminescence vs voltage V_C. Different colors correspond to different G-gate voltages V_G. Vertical dashed lines mark the configuration $V_C = V_G$ for each measurement series. (c) Fitted energy position of the indirect exciton photoluminescence vs voltage V_C at fixed voltage $V_G = -0.6$ V for device T1 (closed circles) and T2 (open circles). Dashed lines mark the Stark shift in the trap/antitrap configurations for device T2, the solid line represents a linear fit for the transition region. (d) Energy tuning ratio $\Delta E/\Delta V_C$ from the linear fit in the transition region measured vs V_G (device T1, closed circles; T2, open circles). Dotted horizontal line marks the slope of the Stark shift in the deep trap ($V_C \ll V_G$).

corresponding to the trap–antitrap transition (marked by the dashed vertical lines in Figure 3a). In turn, the resonances at the antitrap side are blue shifted in energy with respect to the trap side. In a next step, we systematically analyze this blue shift by fitting the excitonic emission energy as a function of V_C for different V_G (Figure 3b). The different colors in Figure 3b correspond to different voltages on the guard gate V_G. We note that for all V_G, the strong blue shift always occurs at the trap–antitrap transition regime.

Generally, a blue shift of the excitonic photoluminescence energy ΔE_X reflects an exciton–exciton interaction-caused increase of the exciton density Δn.[14,17,25,26] It can be estimated to be $\Delta E_X = [(e^2 d_{\vec{p}})/(\varepsilon_s \varepsilon_0)]\Delta n$, with ε_s the dielectric constant of the semiconductor substrate, and $d_{\vec{p}}$ the dipole length, which can be approximated by the distance between the center of the two quantum wells.[27] By varying V_G from +0.5 to −0.6 V, the blue shift increases 2.4 times from 4.04 to 9.64 meV (Figure 3b). For the smaller device T2, it increases 2.3 times (from 5.18 to 11.75 meV, data not shown). These values suggest an increased exciton density of $\Delta n \sim 10^{10}$ cm^{-2} for the antitrap situation, respectively. The interpretation of an increased exciton density in the antitrap compared to a trap is consistent with the observation of abruptly enhanced photoluminescence intensity for the antitrap configuration in Figure 3a. We note that the density enhancement is comparable with the absolute exciton density for $V_G = V_C$, demonstrating significant improvement of the emission efficiency of the device.

We explain the enhanced exciton density for the antitrap configuration by the differences in the escape times from the trap for photogenerated electrons and holes. The electron escape time τ_e can be estimated by the electron velocity ν_d and the drift distance d (trap radius) via $\tau_e = d/\nu_d$. The velocity of electrons depends on a combination of their excess kinetic energy and their drift in the lateral electric field and is estimated to be of order $\sim 10^5 - 10^6$ m/s. The obtained τ_e for the electrons is ~0.01–0.1 ns, and it is an order of magnitude faster than for holes. The electron escape time is thus comparable to the exciton formation time (of the order of 100 ps[28]), and it is significantly faster than the lifetime of indirect excitons (several tens of ns at high vertical electric fields[29]). For a comprehensive description of the evolution of the excitons population, one should also take into account the drift mobility of dipolar excitons, which is $\sim 10^5$ cm^2 V^{-1} s^{-1} in our samples.[30] However, this process is much slower than τ_e, and therefore it cannot compensate the fast escape of photogenerated electrons. In addition, the exciton drift is suppressed in the trapping configuration of the devices. Therefore, it is reasonable to assume that free carrier dynamics significantly influence the emission properties of both the traps and the antitraps.

The presented results clearly demonstrate the importance of these processes when the size of electrostatic excitonic devices is reduced, because then internal in-plane electric fields become even more pronounced. However, we point out that such dynamics give rise to an enhanced electro-optic modulation ratio $\Delta E/\Delta V_C$ at the transition from the trap to the antitrap configuration (dashed region in Figure 3a). In a simple model, we assume that $\Delta E/\Delta V_C$ depends linearly on V_C in the transition region. In Figure 3c, we present an example how the tuning ratio $\Delta E/\Delta V_C$ can be experimentally extracted. We first fit the linear Stark-shift outside of the transition region. Then, we extrapolate the curves into the transition regime (dashed lines). Measurement points which are between these two lines define the transition region. In this region, we obtain the modulation ratio $\Delta E/\Delta V_C$ by a linear fit. We repeat this procedure for different V_G. Figure 3c compares the results for both devices. For device T1, the ratio $\Delta E/\Delta V_C$ increases approximately exponentially with V_G, up to ~73 meV/V at −0.6 V. For the smaller device T2, the energy tuning ratio is even larger, up to ~100 meV/V for $V_G = -0.6$ V. We explain the difference in $\Delta E/\Delta V_C$ for the two devices by an increased exciton density in the smaller device T2. The modulation ratio at the trap/antitrap transition needs to be compared to the ratio of ~30 meV/V for a macroscopic gate geometry based on the linear Stark-effect.[22,24] Indeed, toward the flat-band condition ~0.7 V, all ratios saturate at the value of the bare Stark shift of ~30 meV/V (dotted line in Figure 3d). We would like to note that for very small voltage ranges the ratio $\Delta E/\Delta V_C$ exceeds the linear approximation and another procedure is required to determine the maximum energy tuning parameter (see Supporting Information, Section S4).

Figure 4a presents the influence of V_C on the IX intensity for a fixed V_G. For medium guard voltages $|V_G| < 0.2$ V and small modulations regimes $\Delta V_C \sim 0.1$ V, the intensity changes only by 5%. Thus, it is possible with our device to achieve large energy modulation ratio $\Delta E/\Delta V_C$ at a constant intensity of the emission. We note that the IX emission is continuously tunable in the energy range of 1.535 to 1.58 eV without the appearance of a remarkable resonance, which would indicate waveguide modes with a distinct mode energy. Cavity effects caused by the light interference in heterostructures manifest themselves as a substructure in the photoluminescence spectra, which is revealed in the form of equidistant shoulders as discussed for

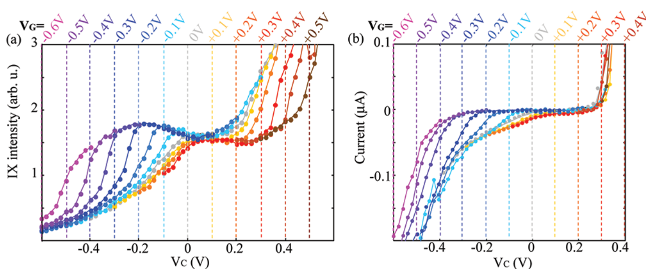

Figure 4. (a) Fitted integrated intensity of the indirect exciton photoluminescence vs voltage V_C. (d) Current between the C- and G-gates versus gate voltage V_C. Different colors correspond to different G-gate voltages V_G. Vertical dashed lines mark the configuration $V_C = V_G$ for each measurement series.

InGaAs double quantum wells.[31] In the measurements presented here, we do not see any signatures of such optical interferences in the PL line shape (see Figure 1d). Further experiments on InGaAs double quantum wells[9] enabled us to study the in-plane propagation of both direct and indirect excitons along a similar device geometry as used here. These studies let us conclude that wave guiding effects and self-absorption caused by the lateral device geometry are not important for the discussed energy modulation effects. The fairly weak modification of the emission intensity at moderate voltages suggests excitonic devices to be advantageous for electro-optic applications. For $|V_C| > 0.2$ V, the intensity varies in a stronger manner (Figure 4a). Partially this can be explained by the vertical electric fields which strongly affects the radiative recombination efficiency of the indirect excitons.[29,32] In addition, the exciton density contributes to the photoluminescence intensity in the microtrap devices. We further notice that a photocurrent is observed for these voltage configurations (Figure 4b). Hereby, the emission intensity is finally reduced because of the ionization of excitons.

In conclusion, we introduce the concept for a nanoscale, exciton-based electro-optical device, which produces a trapping/antitrapping potential for dipolar excitons. We demonstrate high tunability of the emission energy, which is achieved by means of the combination of the Stark effect and dipole–dipole exciton interactions. Thanks to the nanofabrication of the device, the energy tuning ratio was enhanced up to ∼100 meV/V, compared to the bare Stark shift slope ∼30 meV/V. For appropriately chosen voltage configurations, the emission intensity is nearly independent of emission energy. We observe that for downscaling the device dimensions, the emission properties are determined to a large extent by the interactions between photogenerated carriers and excitons in electric fields on a submicrometer scale.

■ ASSOCIATED CONTENT

Supporting Information

Sample structure, device fabrication, and experimental details. Control experiment: trap–antitrap transition under non-resonant and quasi-resonant excitation; maximum energy modulation ratio of the device in a small voltage regime. This material is available free of charge via the Internet at http://pubs.acs.org.

■ AUTHOR INFORMATION

Corresponding Author

*E-mail: k.kowalik@physik.uni-muenchen.de.

■ ACKNOWLEDGMENTS

We thank S. Manus for technical help. We gratefully acknowledge financial support from DFG project KO 416/17, the Center for Nano-Science (CeNS), the "Nanosystems Initiative Munich (NIM)" and "LMUexcellent". K.K.-S. thanks the Alexander von Humboldt Foundation for support.

■ REFERENCES

(1) Keldysh, L. V.; Kozlov, A. N. *Zh. Eksp. Teor. Fiz.* **1968**, *54*, 978; *Sov. Phys.-JETP* **1968**, *27*, 521.
(2) Blatt, J. M.; Böer, K. W.; Brandt, W. *Phys. Rev.* **1962**, *126*, 1691.
(3) Butov, L. V.; Lai, C. W.; Ivanov, A. L.; Gossard, A. C.; Chemla, D. S. *Nature* **2002**, *417*, 47.
(4) Negoita, V.; Snoke, D. W.; Eberl, K. *Phys. Rev. B* **2000**, *61*, 2779.
(5) Christianen, P. C. M.; Piazza, F.; Lok, J. G. S.; Maan, J. C.; van der Vleuten, W. *Physica B* **1998**, *249*, 624.
(6) Hagn, M.; Zrenner, A.; Böhm, G.; Weimann, G. *Appl. Phys. Lett.* **1995**, *67*, 232.
(7) Hammack, A. T.; Gippius, N. A.; Yang, S.; Andreev, G. O.; Butov, L. V.; Hanson, M.; Gossard, A. C. *J. Appl. Phys.* **2006**, *99*, 066104.
(8) Gärtner, A.; Prechtel, L.; Schuh, D.; Holleitner, A. W.; Kotthaus, J. P. *Phys. Rev. B* **2007**, *76*, 085304.
(9) Schinner, G. J.; Schubert, E.; Stallhofer, P. M.; Kotthaus, J. P.; Schuh, D.; Rai, A. K.; Reuter, D.; Wieck, A. D.; Govorov, A. O. *Phys. Rev. B* **2011**, *83*, 165308.
(10) High, A. A.; Hammack, A. T.; Butov, L. V.; Mouchliadis, L.; Ivanov, A. L.; Hanson, M.; Gossard, A. C. *Nano Lett.* **2009**, *9*, 2094.
(11) Zimmermann, S.; Wixforth, A.; Kotthaus, J. P.; Wegscheider, W.; Bichler, M. *Science* **1999**, *283*, 1292.
(12) Lundstrom, T.; Schoenfeld, W.; Lee, H.; Petroff, P. M. *Science* **1999**, *286*, 2312.
(13) Winbow, A. G.; Hammack, A. T.; Butov, L. V.; Gossard, A. C. *Nano Lett.* **2007**, *7*, 1349.
(14) Leonard, J. R.; Kuznetsova, Y. Y.; Yang, Sen; Butov, L. V.; OstatVnick, T.; Kavokin, A.; Gossard, A. C. *Nano Lett.* **2009**, *9*, 4204.
(15) Kowalik-Seidl, K.; Vögele, X. P.; Rimpfl, B. N.; Manus, S.; Kotthaus, J. P.; Schuh, D.; Wegscheider, W.; Holleitner, A. W. *Appl. Phys. Lett.* **2010**, *97*, 011104.
(16) High, A. A.; Hammack, A. T.; Butov, L. V.; Hanson, M.; Gossard, A. C. *Opt. Lett.* **2007**, *32*, 2466.
(17) High, A. A.; Novitskaya, E. E.; Butov, L. V.; Hanson, M.; Gossard, A. C. *Science* **2008**, *321*, 229.
(18) Grosso, G.; Graves, J.; Hammack, A. T.; High, A. A.; Butov, L. V.; Hanson, M.; Gossard, A. C. *Nat. Photonics* **2009**, *3*, 577.
(19) Rapaport, R.; Chen, G; Simon, S.; Mitrofanov, O.; Pfeiffer, L.; Platzman, P. M. *Phys. Rev. B* **2005**, *72*, 075428.
(20) Xu, Q.; Schmidt, B.; Pradhan, S.; Lipson, M. *Nature* **2005**, *435*, 325.
(21) Chen, Y. J.; Koteles, E. S.; Elman, B. S.; Armiento, C. A. *Phys. Rev. B* **1987**, *36*, 4562.
(22) Kowalik-Seidl, K.; Vögele, X. P.; Seilmeier, F.; Schuh, D.; Wegscheider, W.; Holleitner, A. W.; Kotthaus, J. P. *Phys. Rev. B* **2011**, *83*, 081307(R).
(23) Gerardot, B. D.; Seidl, S.; Dalgarno, P. A.; Warburton, R. J.; Kroner, M.; Karrai, K.; Badolato, A.; Petroff, P. M. *Appl. Phys. Lett.* **2007**, *90*, 221106.
(24) This value is in a good agreement with the slope 33 meV/V obtained from numerical simulations in such a heterostructure using the software Nextnatno3 (http://www.nextnano.de). Note that the slope of the Stark shift might be reduced, when the applied electric field is screened by the high density of dipolar excitons (see ref 22).
(25) Zimmermann, R.; Schindler, C. *Solid State Commun.* **2007**, *144*, 395.
(26) Laikhtman, B.; Rapaport, R. *Phys. Rev. B* **2009**, *80*, 195313.
(27) Rapaport, R.; Chen, G.; Simon, S. H. *Phys. Rev. B* **2006**, *73*, 033319.
(28) Damen, T. C.; Shah, J.; Oberli, D. Y.; Chemla, D. S.; Cunningham, J. E.; Kuo, J. M. *Phys. Rev. B* **1990**, *42*, 7434.

(29) Alexandrou, A.; Kash, J. A.; Mendez, E. E.; Zachau, M.; Hong, J. M.; Fukuzawa, T.; Hase, Y. *Phys. Rev. B* **1990**, *42*, 9225.
(30) Gärtner, A.; Holleitner, A. W.; Kotthaus, J. P.; Schuh, D. *Appl. Phys. Lett.* **2006**, *89*, 052108.
(31) Schinner, G. J.; Repp, J.; Schubert, E.; Rai, A. K.; Reuter, D.; Wieck, A.; Govorov, A. V.; Holleitner, A. W.; Kotthaus, J. P. ArXiv:1111.7175v1, 2011.
(32) Ivanov, A. L. *J. Phys.: Condens. Matter* **2004**, *16*, S3629.